

The tangential velocity of M31: CLUES from constrained simulations

Edoardo Carlesi,¹ * Yehuda Hoffman,¹ Jenny G. Sorce,² Stefan Gottlöber,² Gustavo Yepes,^{5,6} H            ,³ R. Brent Tully⁴

¹*Racah Institute of Physics, Givat Ram, 91040 Jerusalem, Israel*

²*Leibniz-Institut f  r Astrophysik Potsdam (AIP), An der Sternwarte 16, D-14482 Potsdam, Germany*

³*University of Lyon, UCB Lyon 1/CNRS/IN2P3, F-69007 Lyon, France*

⁴*Institute for Astronomy (IfA), University of Hawaii, 2680 Woodlawn Drive, HI 96822, US*

⁵*Grupo de Astrof  sica, Departamento de F  sica Te  rica, Modulo C-8, Universidad Aut  noma de Madrid, E-280049 Cantoblanco, Spain*

⁶*Astro-UAM, UAM, Unidad Asociada CSIC, E-280049 Cantoblanco, Spain*

Submitted XXXX January XXXX

ABSTRACT

Determining the precise value of the tangential component of the velocity of M31 is a non trivial astrophysical issue, that relies on complicated modeling. This has recently lead to conflicting estimates, obtained by several groups that used different methodologies and assumptions. This *letter* addresses the issue by computing a Bayesian posterior distribution function of this quantity, in order to measure the compatibility of those estimates with Λ CDM. This is achieved using an ensemble of local group (LG) look-alikes collected from a set of Constrained Simulations (CSs) of the local Universe, and a standard unconstrained Λ CDM. The latter allows us to build a control sample of LG-like pairs and to single out the influence of the environment in our results. We find that neither estimate is at odds with Λ CDM; however, whereas CSs favour higher values of v_{tan} , the reverse is true for estimates based on LG samples gathered from unconstrained simulations, overlooking the environmental element.

Key words: methods: N -body simulations – galaxies: haloes – cosmology: theory – dark matter

1 INTRODUCTION

The knowledge of the proper motion of M31 is required in order to constrain the properties and the evolution of the Local Group (LG). Though the radial component of the velocity vector has been obtained more than one hundred years ago, the measure of its tangential velocity, v_{tan} , is a much more challenging task. In fact its value needs to be extrapolated through complicated modelling and under several hypotheses about the kinematics of satellite galaxies and its stellar populations.

A major breakthrough in this regard was represented by the work of van der Marel & Guhathakurta (2008) that was able to put an upper limit of 56 km s^{-1} to the transverse velocity of the M31 system from the line-of-sight motion of its satellites, assuming that they would on average follow their host galaxy. Sohn et al. (2012) were able to provide the first reconstruction of the M31 velocity vector itself, yielding a value of $17 \pm 17 \text{ km s}^{-1}$ for its tangential component. This was done by measuring the displacement of different stellar populations within M31 with respect to reference

galaxies in the background, using some complicated modeling to single out the motion of the stars within M31 from the motion due to M31 itself. However, these results have been recently challenged by Salomon et al. (2016), that using the precise measurements of satellite galaxy distances of Conn et al. (2012), obtain a value of $v_{\text{tan}} = 164 \pm 61 \text{ km s}^{-1}$, at odds with the aforementioned analysis. In the following, the estimates of Sohn et al. (2012) and Salomon et al. (2016) will be referred to as $v_{\text{tan}}^{(I)}$ and $v_{\text{tan}}^{(II)}$ respectively.

A different approach is followed here, which is based on a Bayesian inference of the value of v_{tan} . Such an inference starts with a prior knowledge of the system at hand and a set of observations that are used to improve our knowledge of the tangential velocity of M31. This improved knowledge constitutes the posterior probability of v_{tan} given the prior knowledge and the observations. The inference of v_{tan} is based on the sampling of the posterior probability distribution function. The prior knowledge is split here into two independent models. One is the standard cosmological model that describes the Universe at large - and here the Λ CDM model is assumed. The other is the LG model. Namely, it needs to be assumed a priori what is a LG. The model can consist of the basic dynamical characteristics of the LG, such as the distance and

* E-mail: carlesi@phys.huji.ac.il

relative radial velocity of a pair of halos and their isolation. The model can be extended to include information about the merging history of the pairs of halos. The Cosmicflows-2 dataset of peculiar velocities (CF2, Tully et al. 2013) serves here as the observational data on our local 'patch' of the Universe. The non-linear nature of the LG renders the analytical approach impossible and numerical simulations are to be used for sampling the likelihood and posterior probability distribution functions. Constrained simulations are used to provide non-linear realizations of which obey both the prior Λ CDM model and CF2 data (Sorce 2015; Carlesi et al. 2016a). The ensemble of LG-like objects that emerge from the CF2 constrained simulations and the LG model provides a numerical sampling of the posterior probability. The ensemble of LGs constructed from random simulations and the LG model sample the prior (likelihood) probability.

In this *letter* we calculate the posterior probability of the transverse velocity of the M31 galaxy (v_{tan}), assuming the Λ CDM model and given the CF2 data. This work is structured as follows. The likelihood function of v_{tan} in a Λ CDM universe is calculated as well and is compared with the posterior function. Section 2 describes the prior cosmological model, the model used to define a LG and the (constrained and random) simulations. The posterior distribution and the likelihood functions are presented in Section 3. A summary and an assessment of the implications of the results for the estimations of v_{tan} (Sohn et al. 2012; Salomon et al. 2016) are given in Section 4.

2 METHODS

Prior cosmological model: The prior model is assumed here to be standard Λ CDM with the Planck-I cosmological parameters of $\Omega_m = 0.31$, $\Omega_\Lambda = 0.69$, $h = 0.67$ and $\sigma_8 = 0.83$ (Planck Collaboration et al. 2014). A non-linear realization of the model is provided by the CurieHZ project¹ and consists in a (DM) only simulation done in a box size of $200h^{-1}$ Mpc with 1024^3 particles, which will be referred to as Rand hereafter. DM halos are extracted from the simulation by the AHF halo finder (Knollmann & Knebe 2009) with halo mass defined by M_{200} (with respect to ρ_c). The choice of this mass definition has only but a minor impact on v_{tan} as we checked by comparing to the results obtained with M_{vir} , the mass at the viral radius.

Prior LG model: Some of the fairly indisputable observational facts that describe the LG are the distance and relative radial velocity (v_{rad}) between the MW and M31 galaxies and the lack of a third comparable companion within a distance of 3 Mpc. This leads us to formulate a very simplified prior model of the LG. An isolated pair of halos separated by a distance of $(0.35 - 0.70)h^{-1}$ Mpc and with v_{rad} in the range of $(-135 - -80)$ km s^{-1} , is defined be a LG like object. Isolation is defined by the absence of a halo more massive than the least massive of the two within $2.5h^{-1}$ Mpc. The ranges of v_{rad} and r are within $\pm 25\%$ of the fiducial values taken from van der Marel et al. (2012). The prior model reflects the prior knowledge, or sometime prejudice, one has on the system at hand. The mass of the LG is far from being precisely known and estimates of it ranges over a factor of a few. Here we are willing to entertain the idea of introducing a mass range into the LG model. In the following we shall use two LG models, or priors; one with no mass constraints and one in which mass of the LG (defined as

Table 1. Kinematic priors on radial velocities (in km s^{-1} units) and relative distances of the haloes (in h^{-1} Mpc); mass priors are given in $10^{12}h^{-1}M_\odot$ units. N_{CS} and N_{Rand} are the numbers of halo pairs satisfying the criteria in the samples drawn from CS and Rand simulations.

V_{rad}	r	M_{LG}	N_{CS}	N_{Rand}
$[-135, -80]$	$[0.35, 0.70]$	-	1004	857
$[-135, -80]$	$[0.35, 0.70]$	$[0.5, 5.0]$	173	365

the sum of the M_{200} of the two main haloes) ranges over $(0.5 - 5.0)h^{-1}M_\odot$ (see Table 1). That mass range reflects the uncertainties in various attempts to estimate the mass of the LG (see e.g. Klypin et al. 2002; Widrow & Dubinski 2005; Li & White 2008; Karachentsev et al. 2009; van der Marel et al. 2012).

CF2 data and Constrained simulations: The bulk of the work described here relies on a set of 500 DM-only zoom simulations generated using the Local Group Factory (Carlesi et al. 2016a). The Local Group Factory is a numerical pipeline designed for the production of N -body zoom simulations of LG-like objects within a large scale environment (Virgo, filament and Local Void) that closely matches the observational one. The initial conditions for these simulations are generated using peculiar velocity data (taken from the CF2 catalog of Tully et al. (2014)) as constraints; for a detailed description of the physical and mathematical aspects of the CS technique we refer to the works of Doumler et al. (2013a,b,c) and Sorce et al. (2014, 2016). The cosmology used is of the Planck-I type, as in the case of the Rand simulation, whereas the particle mass in the high resolution region is $m_p = 6.57 \times 10^8 h^{-1}M_\odot$. Our second sample (labeled CS) can straightforwardly obtained applying the aforementioned LG prior model to our set of CS simulations, ensuring that all of these objects live within an environment whose main features are remarkably close to the actual one.

Sampling The sampling of the posterior distribution and the likelihood functions of v_{tan} of the M31 follows the procedure used by Busha et al. (2011) and (González et al. 2014) for the estimation of the mass of the MW and the LG, respectively. We select ensembles of pairs of halos which obey the LG model from CF2-constrained and from random Λ CDM simulations; these samples provide numerical realizations of the posterior probability and the likelihood functions. In the case of the likelihood function the search for the LGs extends over the full computational box, where in the posterior case the search is conducted within a sphere of $7h^{-1}$ Mpc around the box center for each realization. These realizations are used to calculate the mean and scatter of v_{tan} and to provide analytical fits to the above distribution function. The sampling of the posterior distribution and the likelihood functions is performed twice - without and with the LG mass prior.

3 PRIOR AND POSTERIOR PROBABILITY OF THE TANGENTIAL VELOCITY

The four variants of the posterior probability introduced in the previous paragraph are shown in Fig. 1. Taking the \log_{10} of v_{tan} it is possible to see that these distributions are well matched by a Gaussian function:

$$f(\log_{10} v) = \frac{1}{\sqrt{2\pi}\sigma} \exp - \frac{(\log_{10} v - \mu)^2}{2\sigma^2} \quad (1)$$

¹ <http://curiehz.ft.uam.es/>

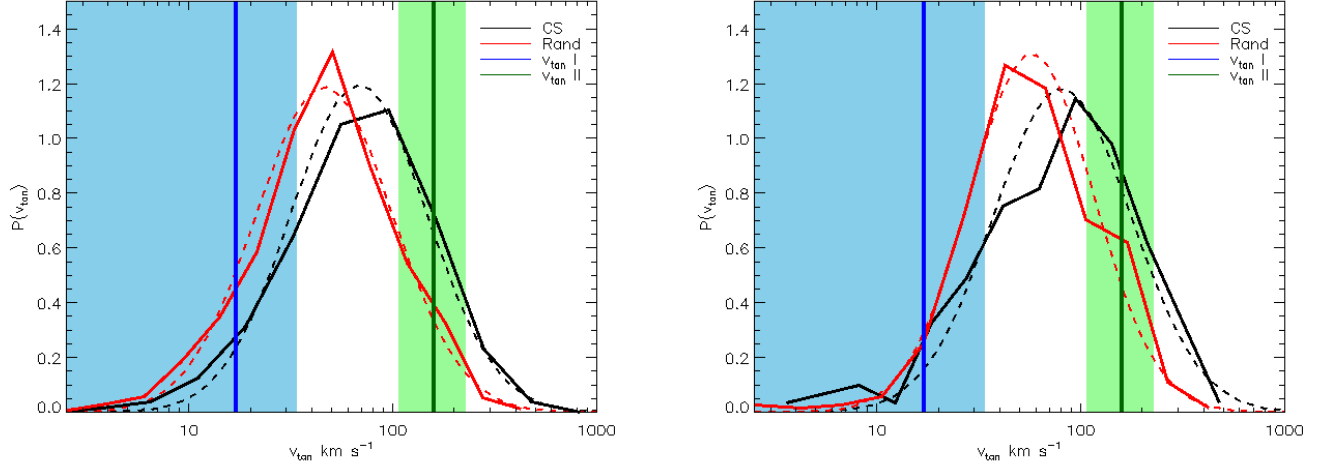


Figure 1. v_{tan} distributions (thick lines) and fits to a log-normal distribution (dashed lines) for the CS and Rand samples. Left panel: Table 1, with no M_{LG} prior. Right panel: same priors with $M_{LG} = [0.5, 5] \times 10^{12} h^{-1} M_{\odot}$. The vertical blue line stands for the $v_{\text{tan}}^{(I)}$ value while the green one for $v_{\text{tan}}^{(II)}$; the shaded areas around them indicate the 1σ intervals.

Table 2. Mean and standard deviations of the $\log_{10}(v_{\text{tan}})$ distribution. The table contains numerical (μ_N and σ_N) and best fit values to a Gaussian function (μ and σ), a different set of priors on radial velocity and relative distance.

Sample	μ_N	σ_N	μ	σ	M Prior
CS	1.97	0.36	1.89	0.34	NO
Rand	1.77	0.35	1.71	0.33	NO
CS	1.97	0.36	1.89	0.33	YES
Rand	1.77	0.35	1.72	0.32	YES

Table 3. Fiducial values with $\pm\sigma$ upper and lower values for $v_{\text{tan}}^{(I)}$, $v_{\text{tan}}^{(II)}$ and theoretical best-fit value estimates from the CS and Rand simulations (analytical estimate, no mass priors), in units of km s^{-1} .

	v	$v + \sigma_v$	$v - \sigma_v$
$v_{\text{tan}}^{(I)}$	17	34	0
$v_{\text{tan}}^{(II)}$	164	225	103
v_{tan}^{CS}	78	168	36
v_{tan}^{Rand}	51	109	24

whose resulting means and standard deviations, for both the numerical and analytical best fit values, are shown in Table 2.

In general, one can test the sensitivity of the $P(v_{\text{tan}})$ to the choice of the interval, repeating the above computation using larger (narrower) selection intervals on v_{rad} and r . This is true also when adding mass constraints, that have the only effect of substantially reducing the size of the sample, without altering the properties of the posterior distribution function. The results of these tests, which are presented in Appendix A, confirm that the distributions are at best weakly sensitive on the priors, similarly to what González et al. (2014) have found in the case of the $P(M_{LG})$.

These posterior distribution functions yield the theoretical v_{tan} s, which are compared to the observational ones in Table 3, where it is shown that both v_{tan} s are in substantial agreement with

ΛCDM and $\Lambda\text{CDM}+\text{CF2}$ predictions. In fact, the overlap between the 2σ intervals is nonzero, even though the peaks of $P(v_{\text{tan}})$ for the two samples tend to be far from both $v_{\text{tan}}^{(I)}$ and $v_{\text{tan}}^{(II)}$. To calculate the compatibility of the two estimates with the theoretical predictions, that is their posterior probability or degree of belief, we compute the integral:

$$\int_{v_0 - \Delta v}^{v_0 + \Delta v} dv' f(v') \quad (2)$$

where $f(v')$ is the Gaussian of Eq. (1), σ and μ are the best fit values of Table 2 and v_0 is given by the \log_{10} values of $v_{\text{tan}}^{(I)}$ and $v_{\text{tan}}^{(II)}$. The intervals Δv are chosen to be the 1σ values relative to $v_{\text{tan}}^{(I)}$ and $v_{\text{tan}}^{(II)}$ (see Table 3). The numerical equivalent of the integral is simply given by

$$P_{I,II}^{(N)} = \frac{N_{v \pm \Delta v}}{N_{\text{tot}}} \quad (3)$$

where N_{tot} is the total number of LG pairs of the sample and $N_{v \pm \Delta v}$ is the number of haloes within the intervals around the fiducial v_{tan} s.

The results of these calculations are shown in Table 4, showing that $P_I > P_{II}$ for the Rand simulations and $P_I < P_{II}$ in the case of the CS set, consistently for both numerical and analytical estimates. Moreover, the ratio of the two probabilities indicates that whereas $v_{\text{tan}}^{(I)}$ would be favoured by *vanilla* ΛCDM , with $\frac{P_I}{P_{II}} > 1.27$, the opposite is true when adding environmental constraints (as given by the CF2 data). In the latter case, in fact, the probabilities are reversed and the ratio $\frac{P_I}{P_{II}} < 0.5$ indicates that $v_{\text{tan}}^{(II)}$ kind of velocities are favoured when considering a LG pairs within a more realistic reconstruction of the Universe.

4 CONCLUSIONS

This work provides the posterior probability of the tangential velocity (v_{tan}) of the M31 galaxy assuming the ΛCDM standard model

Table 4. Probabilities of $v_{\text{tan}}^{(I)}$ and $v_{\text{tan}}^{(II)}$ for CS and Rand LG samples and the different prior sets. P_I^A, P_{II}^A refer to the analytical estimates computed via Eq. (2), while P_I^N, P_{II}^N are the numerical values, derived as the fractions of pairs within those intervals. Remarkably, these latter values are completely unchanged by the restriction of M_{LG} values, despite the large shrink in the halo sample size.

Sample	P_I^A	P_{II}^A	P_I^N	P_{II}^N	M_{LG} Prior
CS	0.14	0.28	0.12	0.34	NO
Rand	0.29	0.16	0.23	0.18	NO
CS	0.14	0.29	0.12	0.34	YES
Rand	0.27	0.16	0.23	0.18	YES

of cosmology, a LG model which defines what is a LG, and given the Cosmicflows-2 database of peculiar velocities. This is compared with the likelihood function of v_{tan} given the prior Λ CDM and the LG models. The sampling of the posterior probability and the likelihood function is done by extracting all LG-like objects from an ensemble of CF2 constrained Λ CDM simulations via the so-called Local Group Factory (Carlesi et al. 2016a) and from a random Λ CDM simulation, respectively. A simple LG model which specifies the distance, relative radial velocity and the degree of isolation of a pair of halos is used to extract the LG-like objects. We used numerical and best-fit analytical expressions to derive *predictions* of Λ CDM model (and Λ CDM+CF2 data, in the case of CS) for v_{tan} . Posterior probabilities for $v_{\text{tan}}^{(I)}$ and $v_{\text{tan}}^{(II)}$ (defined as the v_{tan} obtained by Sohn et al. (2012) and Salomon et al. (2016)) were also computed, integrating the distributions over the 1σ v_{tan} intervals of the two observations.

The main findings can be summarized as follows:

- The posterior probability and the likelihood function are both well approximated by a lognormal distribution (with respect to $\log v_{\text{tan}}$). The posterior probability and the likelihood function are quite similar, with a small offset of their parameters.
- The mean and standard deviations for v_{tan} are 78_{-42}^{+90} km s⁻¹ for the posterior distribution (i.e. CF2-constrained simulations, CS) and 51_{-27}^{+58} km s⁻¹ for prior Λ CDM model (i.e. the Rand simulation).
- Both $v_{\text{tan}}^{(I)}$ and $v_{\text{tan}}^{(II)}$ estimates are in agreement with the posterior distribution and the prior Λ CDM model to within the 2σ compatibility range. However, it was consistently found that Λ CDM+CF2 tends to favour $v_{\text{tan}}^{(II)}$ over $v_{\text{tan}}^{(I)}$ whereas the reverse is true for Λ CDM-only based estimates.
- The present results are largely insensitive to the choice of priors. We have shown that both the posterior probability and the likelihood function are very weakly affected by modification of the LG-samples induced by altering the LG model used here. This includes a very small sensitivity to the assumed mass range of the LG. This result is akin to the one found by González et al. (2014), using a similar approach for the MW mass.

So, while both $v_{\text{tan}}^{(I)}$ and $v_{\text{tan}}^{(II)}$ values are possible outcomes of prior Λ CDM and the posterior Λ CDM+ CF2, using constrained and random simulations we showed that the peculiar nature of the LG environment, as manifested by the CF2 data, mildly favours a higher v_{tan} , preferring the Salomon et al. (2016) result over the estimate of Sohn et al. (2012). We conclude by adding that the approach used here, that relies heavily on the use of large samples of CSs produced with the so called Local Group factory, can be extended to analyze and derive posterior distributions for many other

LG properties, such as e.g. satellite populations and mass, which are the subject of current investigation.

ACKNOWLEDGEMENTS

EC would like to thank the Lady Davis Fellowship Fund for financial support. JS acknowledges support from the Alexander von Humboldt foundation. YH has been partially supported by the Israel Science Foundation (1013/12). SG and YH acknowledge support from DFG under the grant GO563/21-1. GY thanks MINECO (Spain) for financial support under project grants AYA2012-31101 and AYA2015-63810-P. We thank the anonymous referee for his useful remarks. We also thank the Red Española de Supercomputación for granting us computing time in the Marenostrum Supercomputer at the BSC-CNS where part of the analyses presented in this paper have been performed, as well as PRACE for granting computing time in the CURIE supercomputer where the CurieHZ simulations was done.

REFERENCES

- Busha M. T., Marshall P. J., Wechsler R. H., Klypin A., Primack J., 2011, *ApJ*, 743, 40
- Carlesi E., Sorce J. G., Hoffman Y., Gottlöber S., Yepes G., Libeskind N. I., Pilipenko S. V., Knebe A., Courtois H., Tully R. B., Steinmetz M., 2016a, *MNRAS*
- Conn A. R., Ibata R. A., Lewis G. F., Parker Q. A., Zucker D. B., Martin N. F., McConnachie A. W., Irwin M. J., Tanvir N., Fardal M. A., Ferguson A. M. N., Chapman S. C., Valls-Gabaud D., 2012, *ApJ*, 758, 11
- Doumler T., Courtois H., Gottlöber S., Hoffman Y., 2013b, *MNRAS*, 430, 902
- Doumler T., Gottlöber S., Hoffman Y., Courtois H., 2013c, *MNRAS*, 430, 912
- Doumler T., Hoffman Y., Courtois H., Gottlöber S., 2013a, *MNRAS*, 430, 888
- González R. E., Kravtsov A. V., Gnedin N. Y., 2014, *ApJ*, 793, 91
- Karachentsev I. D., Kashibadze O. G., Makarov D. I., Tully R. B., 2009, *MNRAS*, 393, 1265
- Klypin A., Zhao H., Somerville R. S., 2002, *ApJ*, 573, 597
- Knollmann S. R., Knebe A., 2009, *ApJS*, 182, 608
- Li Y.-S., White S. D. M., 2008, *MNRAS*, 384, 1459
- Planck Collaboration Ade P. A. R., Aghanim N., Armitage-Caplan C., Arnaud M., Ashdown M., Atrio-Barandela F., Aumont J., Baccigalupi C., Banday A. J., et al. 2014, *A&A*, 571, A16
- Salomon J.-B., Ibata R. A., Famaey B., Martin N. F., Lewis G. F., 2016, *MNRAS*, 456, 4432
- Sohn S. T., Anderson J., van der Marel R. P., 2012, *ApJ*, 753, 7
- Sorce J. G., 2015, *MNRAS*, 450, 2644
- Sorce J. G., Courtois H. M., Gottlöber S., Hoffman Y., Tully R. B., 2014, *MNRAS*, 437, 3586
- Sorce J. G., Gottlöber S., Yepes G., Hoffman Y., Courtois H. M., Steinmetz M., Tully R. B., Pomarède D., Carlesi E., 2016, *MNRAS*, 455, 2078
- Tully R. B., Courtois H., Hoffman Y., Pomarède D., 2014, *Nature*, 513, 71
- Tully R. B., Courtois H. M., Dolphin A. E., Fisher J. R., Héraudeau P., Jacobs B. A., Karachentsev I. D., Makarov D., Makarova L., Mitronova S., Rizzi L., Shaya E. J., Sorce J. G., Wu P.-F., 2013, *AJ*, 146, 86

Table A1. Alternative priors on v_{rad} (in km s^{-1} units), r (in $h^{-1} \text{Mpc}$) and masses (in $10^{12} h^{-1} \text{M}_{\odot}$ units). N_{CS} and N_{Rand} are the numbers of halo pairs for each prior set, for the CS and Rand simulations.

Prior	v_{rad}	r	M_{LG}	N_{CS}	N_{Rand}
Pr.1	$[-120, -100]$	$[0.45, 0.57]$	-	118	113
Pr.2	$[-165, -55]$	$[0.25, 0.78]$	-	1806	4021
Pr.3	$[-120, -100]$	$[0.45, 0.57]$	$[0.5, 5.0]$	22	55
Pr.4	$[-165, -55]$	$[0.25, 0.78]$	$[0.5, 5.0]$	259	1599
Pr.5	$[-165, -55]$	$[0.25, 0.78]$	$[1.0, 3.0]$	184	1167

van der Marel R. P., Fardal M., Besla G., Beaton R. L., Sohn S. T., Anderson J., Brown T., Guhathakurta P., 2012, *ApJ*, 753, 8
 van der Marel R. P., Guhathakurta P., 2008, *ApJ*, 678, 187
 Widrow L. M., Dubinski J., 2005, *ApJ*, 631, 838

This paper has been typeset from a \LaTeX file prepared by the author.

APPENDIX A: LOCAL GROUP MODEL AND POSTERIOR PROBABILITY

In principle, the properties of the posterior probability derived in this work might be dependent on the specific choice of our prior Local Group model, for which many different prescriptions are allowed. The trade-off between sample size and closeness to the observations (in particular with regard to r and v_{rad} , which are strongly constrained by the data) has lead to a choice of intervals of $\pm 25\%$ around the fiducial values.

We will now show that the main results of the paper are largely unaffected by this specific choice of the priors, by repeating the procedures explained in Section 3 with the new LG-like pairs selected according to the new criteria. These are shown in Table A1, where the new values for v_{rad} and r are now taken to be $\pm 2\sigma$ and $\pm 50\%$ around the fiducial values; with and without additional restrictions on the mass. With respect to the results of Table 2, the best fit and numerical μ s and σ s undergo very small changes, and the posterior probability derived using the CS sample keeps peaking at larger values than the one computed using the Rand LG-like haloes. The most important change that can be noticed is the reduction in the standard deviations of the 2σ samples, for the Rand simulations alone. This can be shown to be related to the final mass distribution of the LGs for this choice of the priors. However, this correlation is just mentioned here as its implications are outside the scope of this work, as we plan to discuss it in depth in an upcoming paper.

These findings for the distributions imply that the numerical and analytical probabilities computed with them are expected to give very similar results. This is indeed the case, as can be seen by looking at Table A3, where these numbers are calculated explicitly. We have therefore shown that our results are not biased by the choice of the prior as both more and less restrictive choices lead to the same results.

Table A2. Numerical and best-fit values for the standard deviation σ and mean μ , for the four sets of priors of Table A1.

Sample	μ_N	σ_N	μ	σ
Pr.1, CS	1.99	0.37	1.88	0.35
Pr.1, Rand	1.80	0.28	1.72	0.24
Pr.2, CS	1.94	0.37	1.89	0.34
Pr.2, Rand	1.72	0.40	1.69	0.38
Pr.3, CS	1.99	0.37	1.82	0.35
Pr.3, Rand	1.80	0.28	1.72	0.23
Pr.4, CS	1.94	0.37	1.88	0.33
Pr.4, Rand	1.72	0.40	1.68	0.38
Pr.5, CS	1.90	0.36	1.82	0.30
Pr.5, Rand	1.78	0.34	1.69	0.29

Table A3. Numerical (P^N) and analytical (P^A) posterior probabilities of the 1σ intervals around $v_{\text{tan}}^{(I)}$ and $v_{\text{tan}}^{(II)}$ estimated using numerical and best fit posterior distribution function.

Sample	P_I^A	P_{II}^A	P_I^N	P_{II}^N
Pr.1, CS	0.16	0.27	0.13	0.37
Pr.1, Rand	0.23	0.12	0.18	0.16
Pr.2, CS	0.15	0.28	0.15	0.32
Pr.2, Rand	0.34	0.16	0.30	0.17
Pr.3, CS	0.16	0.27	0.13	0.37
Pr.3, Rand	0.23	0.12	0.18	0.16
Pr.4, CS	0.15	0.28	0.15	0.32
Pr.4, Rand	0.35	0.16	0.30	0.17
Pr.5, CS	0.17	0.23	0.16	0.32
Pr.5, Rand	0.30	0.13	0.21	0.21